AIP | Review of Scientific Instruments

Design and performance of sliced-aperture corrugated feed horn antennas

J. Singal, E. Wollack, A. Kogut, M. Limon, P. Mirel, P. Lubin, and M. Seiffert

Citation: Review of Scientific Instruments **76**, 124703 (2005); doi: 10.1063/1.2148990
View online: http://dx.doi.org/10.1063/1.2148990
View Table of Contents: http://scitation.aip.org/content/aip/journal/rsi/76/12?ver=pdfcov
Published by the AIP Publishing

Design and performance of sliced-aperture corrugated feed horn antennas

J. Singal
University of California, Santa Barbara, Code 665, Building 21, Greenbelt, Maryland 20771

E. Wollack and A. Kogut
NASA Goddard Space Flight Center, Code 665, Building 21, Greenbelt, Maryland 20771

M. Limon and P. Mirel
Science Systems and Applications, Inc., Code 665, Building 21, Greenbelt, Maryland 20771

P. Lubin
University of California, Santa Barbara, Broida Hall, Santa Barbara, California 93106

M. Seiffert
Jet Propulsion Laboratory, 4800 Oak Drive, Pasadena, California 91109

(Received 26 August 2005; accepted 3 November 2005; published online 27 December 2005)

We report on the design of corrugated feed horn microwave antennas at 3.3, 5.6, 7.8, and 10.2 GHz for the absolute radiometer for cosmology, astrophysics, and diffuse emission experiment. These horns have low sidelobe symmetrical beams with 12° full width at half power, and three noteworthy features: a 30° slice at the aperture, a profiled rather than a linear taper, and a slowly varying groove depth along the length of the horn. The profiled taper and varying groove depth provided a narrow beam given the existing physical spatial constraints of the instrument in which the horns are used. The 30° slice was necessary for instrumental considerations and has a minimal effect on the symmetry of the beam. The slice reduces the effective aperture radius and overall length to that corresponding to an unsliced horn with an aperture at roughly the middle of the slice and does not introduce any undesirable effects. © *2005 American Institute of Physics.*
[DOI: 10.1063/1.2148990]

I. INTRODUCTION

The absolute radiometer for cosmology, astrophysics, and diffuse emission (ARCADE 2) experiment will measure the absolute radiometric temperature of the cosmic microwave background at a range of frequencies from 3.3 to 90 GHz, a measurement which can constrain the era of first star formation, the degree of clumping in galactic halos, and the mass, energy, and abundance of exotic dark matter particles in the early universe. The experiment compares the emission from the sky to that of a blackbody calibrator target with seven radiometers. This article describes the design and performance of corrugated scalar feed horn antennas with sliced apertures at 3.3, 5.6, 7.8, and 10.2 GHz. The horns in question couple the radiation to the radiometers, which are high electron mobility transistor- (HEMT) based cryogenic Dicke-switched radiometers.

The experiment flies on a balloon to a height of ~35 km and features a novel design to achieve an absolute temperature measurement with a precision in the 1 mK range. See Kogut *et al.*[1] for a further discussion of the ARCADE program.

Corrugated feed horns are often useful at microwave frequencies because, as opposed to simple dipole or noncorrugated horn antennas, they feature symmetrical beam patterns, where the received power is a function only of the angle from the axis of the horn, low cross-polar response, and low sidelobe response, meaning that the received power from the angles outside of the main beam where the response is locally high is significantly suppressed. This is ideally suited to astronomical radiometer applications such as the ARCADE 2 experiment, where it is important for the horns to have a low sidelobe response in order to minimize radiometric pickup from the instrument and the Earth. The experiment imposed constraints on the horn design, as outlined below, resulting in the necessity of having the sliced, profiled horns described in this article.

In the ARCADE 2 experiment, the horn antennas are mounted at the aperture of an open bucket Dewar and point 30° from zenith. This is done for two reasons: to minimize pickup of emission from the balloon and to view the calibrator target at an oblique angle, which reduces reflections from the target. We reconcile the 30° pointing with the need to maintain a flat aperture by slicing the antennas at a 30° angle across the antenna aperture.

In addition to low sidelobe response, we require beams in which the full width at half power in the main lobe is sufficiently narrow, in order to resolve pointing on the sky and obtain data where emission from the galaxy is not dominant. We want the four horns at the lowest frequencies to have identical beam patterns, and therefore they are roughly scaled versions of one another. The maximum length and aperture size for the largest horn, at 3.3 GHz, are set by the geometry of the instrument, which in turn sets the scale of the other horns. Finally, we need the horns to feature a return loss of at least −30 dB across the entire band.

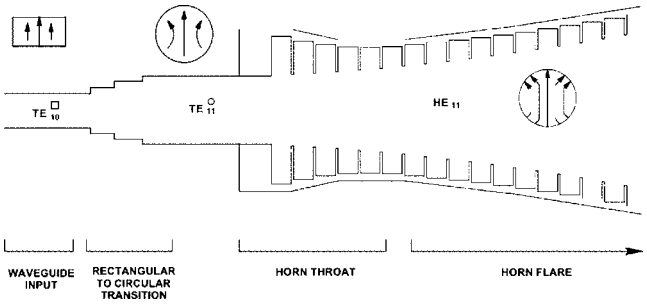

FIG. 1. Schematic of the horn system.

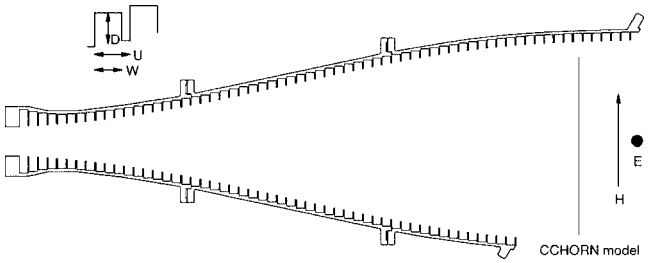

FIG. 2. Profile of the 10 GHz horn as designed, with a close-up showing dimensional parameters. The extent of the modeled unsliced horn is shown, as are the directions of the *E* and *H* planes as referred to in the article.

The center frequencies were chosen for astrophysical interest and the desired fractional bandwidth is ~15% for the four horns in question.

II. HORN DESIGN

As the ARCADE 2 radiometers use standard rectangular waveguide sizes appropriate to the frequency band in question, the horns propagate radiation from a rectangular guide to free space as follows (see Fig. 1): The radiation transitions in a rectangular-to-circular waveguide transition from the TE_{10} mode in a rectangular waveguide to the TE_{11} mode in a circular waveguide with cutoff frequency equal to that of the rectangular guide. This allows for the use of a compact stepped rectangular-to-circular waveguide transition with homogeneous wave propagation in each section.[2] The radius of the throat of the horn is thus fixed at the radius of this circular waveguide.

Figure 2 shows a profile of the horns as designed. We transition from a groove depth of roughly a half wavelength at the throat to a groove depth of roughly a quarter wavelength over the first few tooth and groove cycles. This mode converter converts the TE_{11} circular mode of propagation to the HE_{11} mode.[3] Beyond the mode converter is the flare section, where the groove depth is roughly a quarter wavelength and slowly varies. For ease of manufacturing all of the grooves in a given horn have the same width. If required, the technique of Zhang[4] can be used to achieve a low return loss across a wider band by varying the groove width in the first few sections.

The major effect of the 30° slice on the beam is to reduce the effective aperture radius and overall length to that corresponding to an unsliced horn with an aperture at roughly the middle of the slice. Thus one can predict the behavior of the sliced horns under design by modeling them as shorter, unsliced horns.

In order to achieve an acceptably narrow beam given the aperture size and horn length constraints, we use a tapered rather than a linear profile.[5] The profile of the horn is given by

TABLE I. Parameters.

Channel center frequency (GHz)	Standard waveguide used	Hybrid mode wavelength, λ_x(cm)	Cycle width, U (cm)	Groove width, W(cm)	Number of sections
3.3	WR284	9.3112	2.665	2.3575	56
5.6	WR187	5.3920	1.5432	1.2357	48
7.8	WR112	3.6724	1.0510	0.9298	59
10.2	WR90	3.0392	0.8698	0.7694	59

(a) For all horns profile factor, $(A)=0.839$; transition factor, $(p)=1.843$; number of transition grooves, $(m)=5$; and the cycle width U is the width of one tooth and groove cycle (see Fig. 2).

TABLE II. Specifications.

Channel center frequency (GHz)	Standard waveguide used	Total length (cm)	Total mass (kg)	Aperture major axis (cm)	Aperture minor axis (cm)
3.3	WR284	149	41	67.6	58.7
5.6	WR187	73	11	40.5	35.6
7.8	WR112	62	4	27.3	23.7
10.2	WR90	51	2.5	22.6	19.6

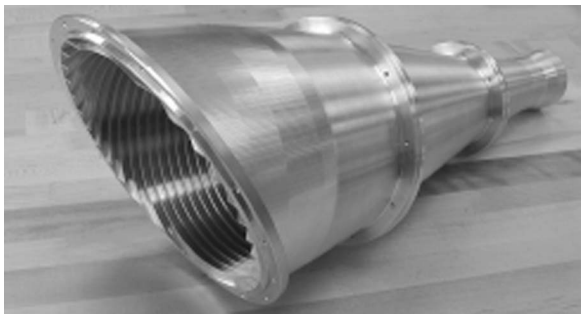

FIG. 3. Photograph of the 10 GHz horn.

$$r = r_t + (r_{\text{apt}} - r_t)\left[(1-A)\frac{z}{L} + A\sin^2(\pi z/2L)\right], \tag{1}$$

with r being the radius corresponding to a distance z along the axis from the throat, L being the total length, r_t being the radius of the throat, r_{apt} being the radius of the aperture, and A being a profile factor.

The groove depth varies along the length of the horn[6] in the flare section according to

$$D_r = \frac{\lambda_x}{4} e^{\lambda_x/5\pi r}, \tag{2}$$

where λ_x is the hybrid mode wavelength, the wavelength where the surface impedance is infinite for the HE_{11} mode. The groove depth is varied in order to allow the HE_{11} mode to adiabatically propagate along the length of the horn.

In the mode converter region, the groove depth of the ith section is given by

$$D_i = D_r + \left(\frac{\lambda_x}{2} - D_r\right)\left(\frac{m-i+1}{m}\right)^p, \tag{3}$$

where m is the number of groove-tooth sections in the transition and p is a transition factor.

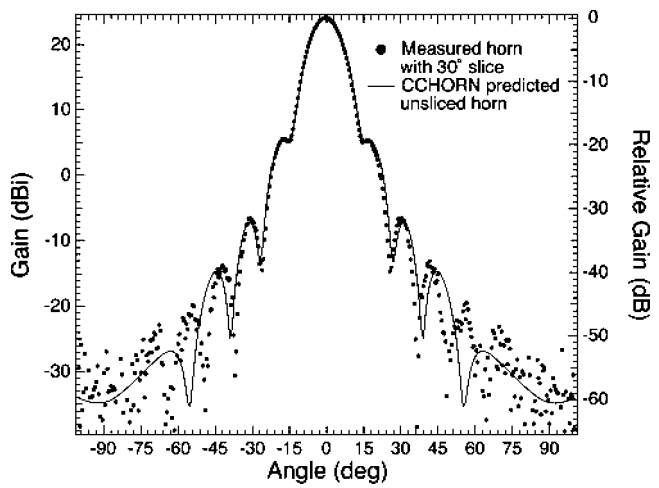

FIG. 4. Predicted and measured E-plane beam pattern for the 10 GHz horn at 10.11 GHz.

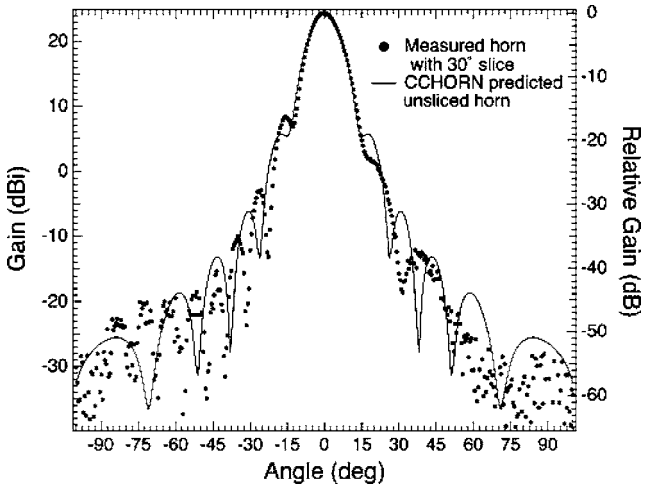

FIG. 5. Predicted and measured H-plane beam pattern for the 10 GHz horn at 10.11 GHz.

We simulate the radiometric performance of the horns under design by modeling unsliced horns using a mode-matching software, CCHORN, based on James.[6] The code treats each tooth or groove section as a separate piece of circular waveguide, solves for the propagation modes available, and matches the boundary conditions with the previous section to solve for the power in each mode.[5,7] Upon reaching the aperture, the modes are summed to give a total electric-field strength and phase distribution, which is then Fourier transformed to give the far-field electric strength and phase distribution.

We determined through the use of an optimization routine that at 3.3 GHz, given the constraints imposed on the overall length and aperture size of the horn by the instrument geometry, the best values for A in order to achieve the narrowest full width at half power, and for p and m, in order to achieve maximal return loss, were 0.839, 1.843, and 5, respectively. For simplicity we applied this to all four horns. The remaining parameters for the other horns were chosen so

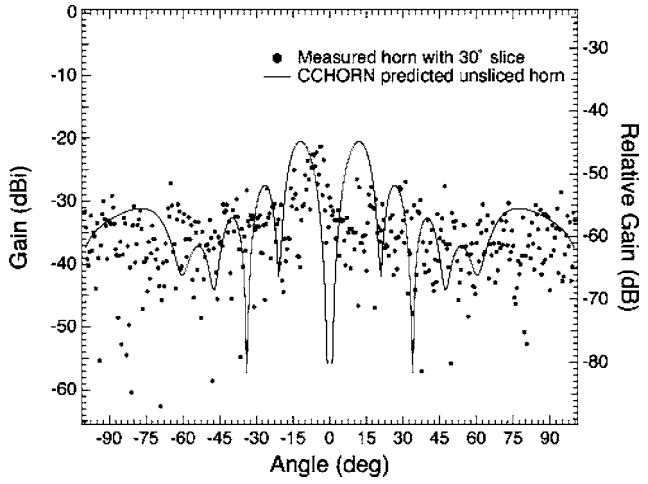

FIG. 6. Predicted and measured cross-polar response for the 10 GHz horn at 10.11 GHz. The measured response is near or below the noise floor of the measurement at most angles.

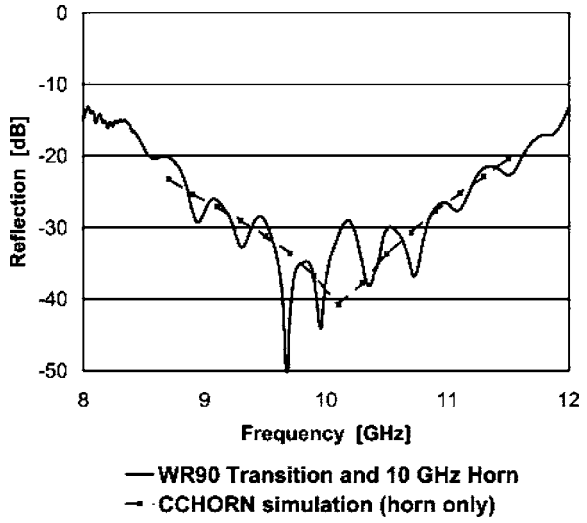

FIG. 7. Predicted reflection loss for the 10 GHz horn and measured reflection loss for the rectangular-to-circular waveguide transition and 10 GHz horn combination.

that the beam patterns were as close as possible to that of the 3.3 GHz horn. Table I lists the values we used for the adjustable parameters for the four horns.

The exterior profiles of the horns were chosen to minimize the overall mass. They are machined in sections out of aluminum. Table II reports the overall scale of the horns. The total length reported is from the throat to the center of the aperture slice. The slice renders the aperture shape itself as approximately an ellipse, and the major and minor axes of that ellipse are reported. Figure 3 shows a photograph of the 10 GHz horn.

III. PERFORMANCE AND EFFECT OF SLICE

We measured the far-field beam pattern of the 10 GHz horn at the Goddard electromagnetic anechoic chamber (GEMAC) compact range. Figures 4 and 5 present the predicted and measured *E*- and *H*-plane beam patterns for the fabricated 10 GHz horn. In the measurement setup used, the *E* and *H* planes are aligned as shown in Fig. 2, with the plane of the aperture slice making a 30° angle with the *E* plane. The effect of the sliced aperture is visible in the *H*-plane cut. Figure 6 shows the cross-polar response and Fig. 7 shows the combined return loss of the horn and circular-to-rectangular waveguide transition combination.

The measured data for the 10 GHz horn indicate that the modeling during the design phase is correct. The other horns should thus have actual beam patterns nearly identical to those predicted.

The dominant observable effect of the slice on the beam pattern is the asymmetry in the *H*-plane response [see Fig. 5], in which the first sidelobe on the side with the slice is suppressed and the first sidelobe level on the opposite side is increased, both by a few decibels.

This asymmetry arises from diffraction effects. In an unsliced horn, or in the *E* plane of the horns in question, the horn aperture is symmetric about the boresight axis, thus in a corrugated feed horn with a symmetrical beam diffraction around the aperture and the effects of this diffraction in the far field are symmetric about this axis. However, in the *H* plane of the sliced horns in question, the aperture of the horn is not symmetric about the boresight axis, and diffraction around the aperture and the far-field effects of this diffraction are correspondingly asymmetric about this axis.

The effect on the main lobe is negligible, and there are no peculiarities in the beam at or near 30° from the boresight, which corresponds to the zenith when the antennas are mounted in the instrument.

ACKNOWLEDGMENTS

The authors thank Dave Reichenthal of Flight Fab Inc. and Thyrso Villela of INPE for fabrication of the horns. This material is based on work supported by the National Aeronautics and Space Administration under Space Astrophysics and Research Analysis program of the Office of Space Science.

[1] A. Kogut, D. J. Fixsen, S. Levin, M. Limon, P. M. Lubin, P. Mirel, M. Seiffert, and E. Wollack, Astrophys. J., Suppl. Ser. **154**, 493 (2004).
[2] G. L. Matthaei, L. P. Young, and E. M. T. Jones, *Microwave Filters, Impedance Matching Networks, and Coupling Structures* (Artech House, Inc., Norwood, MA, 1980).
[3] G. L. James, IEEE Trans. Microwave Theory Tech. **MIT-29**, 1059 (1981).
[4] X. Zhang, IEEE Trans. Microwave Theory Tech. **41-8**, 1263 (1993).
[5] A. D. Olver, P. J. B. Clarricoats, A. A. Kishk, and L. Shafai, *Microwave Horns and Feeds* (IEEE, New York, 1994), pp. 305–307.
[6] G. L. James, IEEE Trans. Antennas Propag. **AP-30**, 1057 (1982).
[7] J. A. Murphy, R. Colgan, C. O'Sullivan, B. Maffei, and P. Ade, Infrared Phys. Technol. **42**, 515 (2001).